Microstructure and diametral fracture strength of spark plasma sintered WC-6Co-0.2B and WC-6Co-0.5B ceramic composites from nanosized and metastable WC powders

G. S. de Alencar e Silva[1], R. M. Leal Neto[2], M. Filgueira[3], C. A. R. P. Baptista[4], C. dos Santos[5]*, A. S. Ramos[1]

[1]*Universidade Federal de Alfenas, Instituto de Ciência e Tecnologia, Poços de Caldas, MG, Brazil*
[2]*Instituto de Pesquisas Energéticas e Nucleares, Centro de Ciência e Tecnologia de Materiais, São Paulo, SP, Brazil*
[3]*Universidade Estadual do Norte Fluminense, Centro de Ciência e Tecnologia, Campos dos Goytacazes, RJ, Brazil*
[4]*Universidade de São Paulo, Departamento de Engenharia de Materiais, Lorena, SP, Brazil*
[5]*Universidade do Estado do Rio de Janeiro, Faculdade de Tecnologia de Resende, Rod. Pres. Dutra, km 298, 27537-000, Resende, RJ, Brazil*

Abstract

The present work aimed at evaluating the microstructures and mechanical properties of spark plasma sintered WC-6 wt% Co ceramic composites doped with boron (0.2 and 0.5 wt%). W-50 at% C (W-6.13 wt% C) powders produced under different milling times (20, 60, 180, and 600 min) were used as starting materials and subsequently mixed with Co (6 wt%) and B (0.2 or 0.5 wt%) powders for 5 min. The resultant WC-Co-B powder mixtures were consolidated by spark plasma sintering at 1450 °C for 10 min at 40 MPa under vacuum in order to obtain the samples with 10 mm diameter and 3 mm thickness. The starting powders and the sintered samples were characterized by laser diffraction particle size analysis, X-ray diffraction with Rietveld refinement, relative density, scanning electron microscopy, energy dispersive spectrometry, Vickers hardness test, and diametral compression test. Supersaturated W solid solution (W_{ss}) with a crystallite size of <50 nm was formed in W-50C (at%) powder mixtures. The relative density of the sintered composites increased with the increasing milling time up to 180 min from 79.7%±0.6% to 86.7%±0.5% for WC-6Co-0.2B and from 86.7%±0.6% to 90.9%±0.4% for WC-6Co-0.5B. Furthermore, the WC phase appeared as the matrix in the sintered samples, and W_2CoB_2 precipitated homogeneously around WC grain boundaries, mainly to those containing 0.5% B. The Vickers hardness values of the sintered WC-6Co-0.2B and WC-6Co-0.5B ranged from 1790±39 to 2158±25 HV and 1858±31 to 2182±28 HV, respectively. The fracture strength (determined by diametral compression test) varied between 144-353 MPa due to the porosity and precipitates in thin-thickness cylinder samples.

Keywords: tungsten carbide-cobalt composites, boron, spark plasma sintering (SPS), Rietveld refinement, mechanical properties.

INTRODUCTION

Tungsten carbide (WC) is a covalent material with high hardness at room temperature (1100-2250 HV) [1], and its high Young's modulus (450-900 MPa) [2] and low thermal expansion coefficient closed to 5.3×10^{-6} °C^{-1} [3] are favorable for machining devices by thermo-mechanical operations. However, due to its low diffusivity, it is difficult to prepare dense WC-based parts by conventional pressureless sintering at temperatures lower than 2000 ºC with longer dwell times, leading to undesirable grain growth and reducing its limited fracture toughness during bending tests. Therefore, high sintering pressures used in hot pressing and liquid-phase sintering can reduce the sintering temperature required to obtain dense WC-based materials by preventing excessive grain growth [4, 5]. In recent years, different alternative routes, including microwave techniques and spark plasma sintering (SPS), have been used for the sintering of WC-based materials. In particular, in comparison to conventional pressureless sintering, SPS is more attractive to produce these denser materials due to its higher heating rate, lower sintering temperature, and shorter dwell time [6, 7]. The SPS process is a field-assisted sintering technique (FAST) in which an external electric field heats a sample and leads to an extremely high heating rate. Extremely high temperatures can be achieved by applying electric pulses of extremely high current densities (around 10,000 A/m²) [8]. Under the conditions of high temperatures and pressures, SPS is applied to sinter ultrafine powders, including low diffusivity materials; thus, the elimination of material porosity can be achieved quickly because ultrafine powders allow a large number of contact points that can form necks [8]. In these necking regions, the applied pressure and electric current generate electric pulses of 1-300 ms; therefore, the rapidly increasing temperature (much higher than those in conventional sintering or hot-pressing processes) completes the densification process in a very short period. When the pulsating discharge appears in the gaps between material particles, a local state of high temperature occurs, and this phenomenon leads to localized vaporization and melting of particles or powder mixtures used in sintering. Consequently, necks are formed around the contact areas between these particles and are developed gradually when the plastic

*https://orcid.org/0000-0002-9398-0639

transformation takes place during sintering, resulting in a sintered compact with a high density. As only the particle surface temperature increases rapidly with self-heating, the grain growth in the material is inhibited, and a more refined microstructure is achieved [6, 8].

Numerous studies [8-11] have correlated the microstructural and mechanical properties of WC-based ceramic composites synthesized by different routes, such as ball milling and SPS. Although the most widely used tests for the determination of fracture strength are three- or four-point bending tests, the tests on transversely loaded thin discs are also used to determine the brittle (tensile) fracture strength of tool materials, such as WC-Co and diamond ceramics [12-14]. It is well known that WC and W_2C (>1250 °C) are the most stable phases in the phase diagram of the W-C system [15], whereas the WC phase can dissolve ~4 at% Co at 1400 °C [16]. The effects of metal addition on the grain growth of WC during sintering as well as the impacts of additives/binders, such as Al_2O_3, Ni_3Al, TiC, B_4C, on the mechanical properties of WC-based ceramic composites have been extensively studied [17-20]. The addition of Ni and Cu (1.2 wt%) can inhibit the growth of plate-like-shaped WC grains and stabilize fcc-Co, whereas Cu can retard the evolution of WC grains from a round to a facetted shape [21, 22]. Different morphologies with triangular and near-hexangular prism shapes can be found in inhomogeneous microstructures of WC-Co ceramics based on coarse and fine WC grains, hindering crack propagation and intergranular fracture [23].

The microstructure of sintered carbides generally contains facetted and abnormally grown grains, and the addition of a small amount of boron (1, 2, and 4 wt%) can induce isotropic coarsening without any abnormal WC grain growth such as to those prepared by spark plasma sintering under vacuum of 4 Pa (or 25 Pa) at a steady heating rate of 150 °C/min and pressure level of 40 MPa from nanosized WC powders (~70 nm). In this study [24], the B_2O_3 phase and W_2C traces were formed at sintering temperatures of up to 1480 and 800 °C, respectively. In addition, the WB formation was identified in samples containing 1 wt% B at sintering temperatures higher than 1480 °C, and its amount increased proportionally to the B content [24]. Moreover, the addition of boron (0.05 wt%) as a sintering additive can reduce the sintering temperature and time in cemented WC-Co ceramics [25]; however, its reactivity during sintering needs to be also investigated. Sugiyama et al. [20] synthesized WC-WB-W_2B composites with no metallic binder from a B_4C-W-WC (molar ratio=1:5:80) powder mixture by solid-state reactions during sintering (1500-1900 °C). Furthermore, previous work [26] found that the Vickers hardness of WC-based ceramics varied from 1800 to 2000 HV and was reduced to 1500-1600 HV after the addition of 5.5 wt% cobalt (WC-5.5Co ceramic composite). The density values of WC-Co-B ceramic were reduced from 12.86 g/cm^3 (for WC ceramic) to 12.57 g/cm^3 (with 0.05 wt% B) and 10.58 g/cm^3 (with 2 wt% B), which were prepared by isostatic pressing (200 MPa) and heating under vacuum (approximately 13.3 Pa) at different sintering temperatures (1250-1440 °C) and times (30-40 min). However, no significant changes in the density (12.42-12.45 g/cm^3) and hardness (15.8-16.1 GPa) values were found for the WC-10Co-0.05B (wt%) ceramic composite previously sintered between 1340 and 1440 °C. Despite the density of close to 12.45 g/cm^3 for the WC-30Ni-0.05 B ceramic composite sintered at 1250-1330 °C for 20 min, the low hardness values close to 6.1 GPa were reported [25]. The present study aimed at evaluating the microstructures and mechanical properties of WC-6Co-0.2B and WC-6Co-0.5B (wt%) ceramic composites densified at low temperatures by the spark plasma sintering (SPS) technique.

MATERIALS AND METHODS

Preparation: W-50C at% (W-6.13C wt%) powder mixtures were produced by high-energy ball milling in a planetary ball mill (P-5, Fritsch, vessel capacity=225 mL, and WC-6Co ball diameter=10 mm) using a rotary speed of 200 rpm with a BPR (ball to powder ratio) of 10:1 from high-purity W (Alfa Aesar, -50+100 mesh, min. 99 wt%) and C (Alfa Aesar, -20+80 mesh, min. 99 wt%) powders under different milling times of 20, 60, 180, and 600 min [27]. In order to investigate the effect of milling time on microstructure and diametral compressive properties of WC-based ceramics, these W-50C at% powders milled at different times were used to prepare the WC-6Co-xB (x= 0.2 and 0.5 wt%) powder mixtures. In this sense, the W-50C (at%) powders previously milled were then mixed with 6 wt% Co (Alfa Aesar, -60 mesh, 99.5 wt%), and 0.2 or 0.5 wt% B (Alfa Aesar, crystalline, +20 mesh, 99.5 wt%) powders in a mill (SPEX 3000M) using a clamp speed of 750 rpm for 5 min in order to obtain homogeneous samples. The resultant WC-6Co-xB powder mixtures were consolidated by spark plasma sintering (SPS) at 1450 °C for 10 min under a low vacuum (between $3.3x10^{-3}$ and $1x10^{-5}$ Pa) in a sintering machine (SPS-211LX Dr. Sinter-Lab, Fuji Elect. Ind.) with a heating rate of 65 °C/min, using a uniaxial pressure of 40 MPa. The powder mixtures were then placed in a graphite cylindrical die with an internal diameter of 10 mm in order to obtain the sintered composite samples with 3 mm thickness. Furthermore, the temperature was measured by placing the radial pyrometer focused on the graphite die. A cooling rate of 200 °C/min up to 800 °C followed by 100 °C/min up to 400 °C and air cooling up to room temperature was used. In order to perform microstructural analyses and mechanical tests, WC-6Co-0.2B and WC-6Co-0.5B ceramic composite specimens (n=5) were produced from the WC powders milled at different times.

Characterization: the particle size distributions of WC-6Co-xB (x= 0.2 and 0.5 wt%) powder mixtures were measured by the laser diffraction particle sizing technique under scattering angle from 0.015° to 144° in an instrument (Mastersizer 2000, Malvern) adopting the Fraunhofer-like particle shape and using water as the dispersing medium. The concentration of the powders suspended in water was lower than 0.02 vol% for an angular range from 0.015° to 144°.

X-ray diffraction (XRD) experiments of the starting materials and the sintered WC-6Co-0.2B and WC-6Co-0.5B ceramic composites were performed in a diffractometer (Empyrean, PANalytical) under the following conditions: diffraction angle (2θ) range=10°-80°, voltage=40 kV, current=30 mA, pass=0.02°/s, and counting time per pass=15 s. JCPDS database files [28] and Rietveld refinement (performed in Fullprof computer program v.2.7.9) [29] were adopted to determine the phase structures, relative contents, lattice parameters of the sintered ceramics, and also the interplanar distances, unit cell volumes, and crystallite sizes of W_{ss} (ss=solid solution) of the as-milled WC starting powders. Furthermore, the amounts of inner and outer pores in the sintered WC-Co-B ceramic composites were measured by the Archimedes principle in water at 25 °C, according to the ASTM B962-14 standard [30] using 14.2 g/cm^3 as the theoretical density obtained by the rule of mixtures. Scanning electron microscopy (SEM) micrographs of W-C-Co-B powder mixtures and the sintered WC-6Co-0.2B and WC-6Co-0.5B ceramic composites were captured by an SEM (TM-3000, Hitachi) equipped with a backscattered electron detector and an energy dispersive spectrometer (EDS) at 15 kV. At least three measurements per phase and inner patterns were adopted for EDS analysis. In order to clarify the elemental distribution in the SPSed samples, the elemental mapping for W, C, Co, and B was conducted by SEM for the SPSed WC-6Co-0.5B ceramic prepared with the W-50C powders milled for 20 min. SEM micrographs of fracture surfaces were obtained by scanning electron microscopy (FEG JSM 7100FT, Jeol, Japan), using a SE detector, 15 kV, WD 10 mm, and SS=6 as parameters. The etched surfaces were carbon-coated using a sputter coater (Emitech K550X, Quorum Technol.-Kent, UK) with 30 mA and 2 min. Vickers hardness tests (Micromet 2100, Buehler, USA) of the sintered WC-6Co-0.2B and WC-6Co-0.5B ceramic composites were conducted according to the ASTM E-384 standard [31] under a load of 500 gf with a loading rate of 0.01 mm/s. The hardness measurements in GPa were also calculated by converting the Vickers hardness number (kgf/mm^2) to SI units, multiplying by the standard gravity (9.80665 m/s^2). Furthermore, the fracture strength of the sintered WC-6Co-0.2B and WC-6Co-0.5B ceramic composites was determined by diametral compression of disk specimens (Brazilian disk test) at room temperature. In this test, the splitting tensile strength of the specimens was calculated according to the ABNT-NBR-7222:11 [32] and ASTM D 3967-16 [33] standards, whose theoretically are based on the solution presented by H. R. Hertz for the elastic stress distribution in a compressed disk. The tests were carried out with a displacement rate of 0.5 mm/s in a testing machine (DL10000, Emic) having 100 kN load capacity and equipped with appropriate compression platens. Sintered specimens with 10 mm diameter and 3 mm height were used in the present work.

RESULTS AND DISCUSSION

Characterization of the W-C-Co-B powder mixtures:

the following JCPDS files were used to index the phases in XRD patterns of W-50C at% powders and sintered samples: W (04-002-1279) [34], graphite-C (04-006-5764) [35], Co (04-002-3693) [36], W_2CoB_2 (04-004-327) [37], and W_3Co_3C (04-010-7467) [38]. Only the presence of W and graphite-C peaks were detected in the XRD patterns of W-50C powders milled for shorter times (20, 60, and 180 min), whereas WC peaks were also identified in the powder milled for 600 min [27]. However, no crystallographic information of phases formed during the ball milling of W-50C powders was obtained by Rietveld refining. Table I shows the effects of milling time on the phase content determined by Rietveld refinement in WC-6Co-xB (x= 0.2 and 0.5 wt%) powder mixtures. Independently on the boron and cobalt amounts added in these powder mixtures, it was noted that the W content promptly increased up to 180 min of milling whereas the C content decreased, suggesting that the C atoms were dissolved into the W lattice in order to form supersaturated solid solutions during ball milling. In addition, the metastability of these powder mixtures was reduced with the partial WC formation in these powder mixtures milled for 600 min. Fig. 1 presents the Rietveld refinement results of the lattice parameter, interplanar distance, unit cell volume, and crystallite size of W_{ss} as a function of milling time. According to Rietveld refining, the lattice parameter of W_{ss} ranged from 3.167 Å (20 min) to 3.157 Å (600 min), whereas its crystallite size was reduced to 45 nm after 600 min of milling. Moreover, the interplanar distance of W_{ss} increased from 2.24 to 2.51 Å due to the interstitial C dissolution in the W lattice. In addition, the FWHM (full width at half maximum) values in severely deformed structures increased from 0.2° to 1.3° with the increasing milling time.

Table I - Effects of milling time on the phase content determined by Rietveld refinement in WC-6Co-xB (x= 0.2 or 0.5 wt%) powder mixtures.

Milling time (min)	W (%)	C (%)	Co (%)	WC (%)
WC-6Co-0.2B				
20	56.1	41.0	2.9	-
60	95.3	2.0	2.7	-
180	98.5	-	1.5	-
600	67.0	-	0.2	32.8
WC-6Co-0.5B				
20	54.0	43.6	2.4	-
60	96.7	1.0	2.3	-
180	98.5	-	1.5	-
600	75.0	-	0.8	23.3

SEM micrographs of W-50C (at%) powder mixtures milled for different times (20, 60, 180, and 600 min) are displayed in Fig. 2. The presence of ductile W particles with
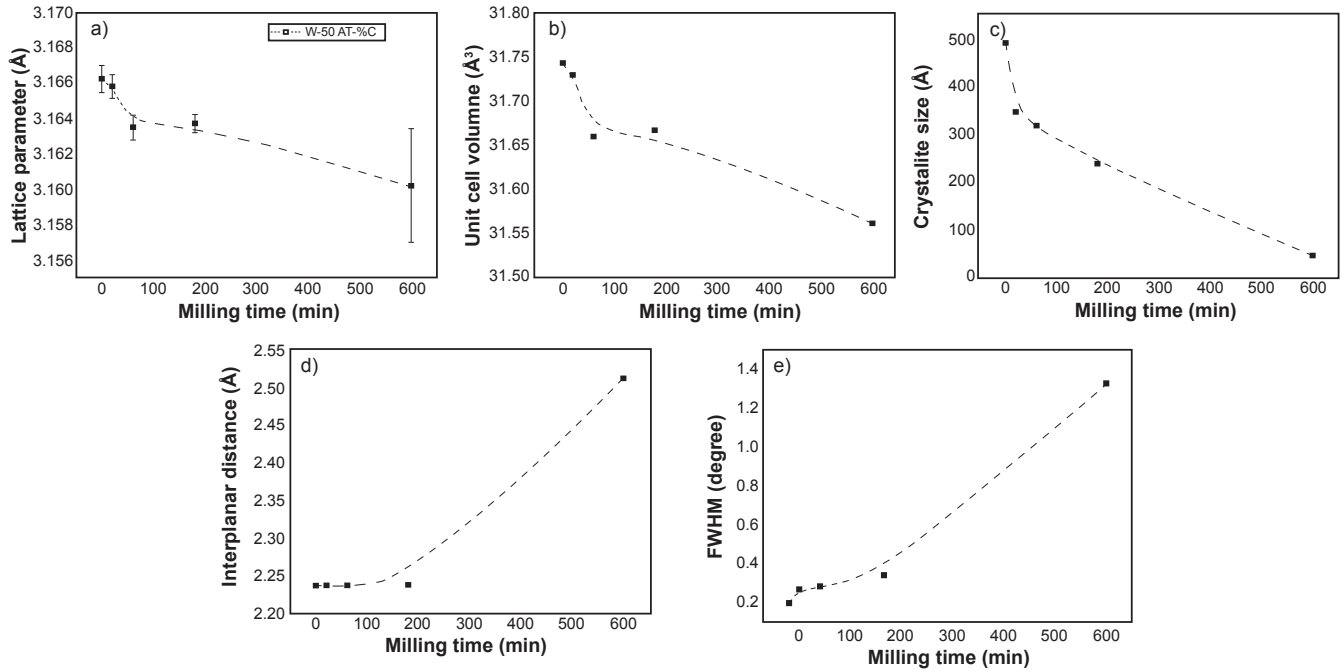
Figure 1: Effect of milling time of W-50C (at%) powder mixture on the crystallographic data of W_{ss} (ss-solid solution): a) lattice parameter; b) unit cell volume; c) crystallite size; d) interplanar distance; and e) FWHM values.
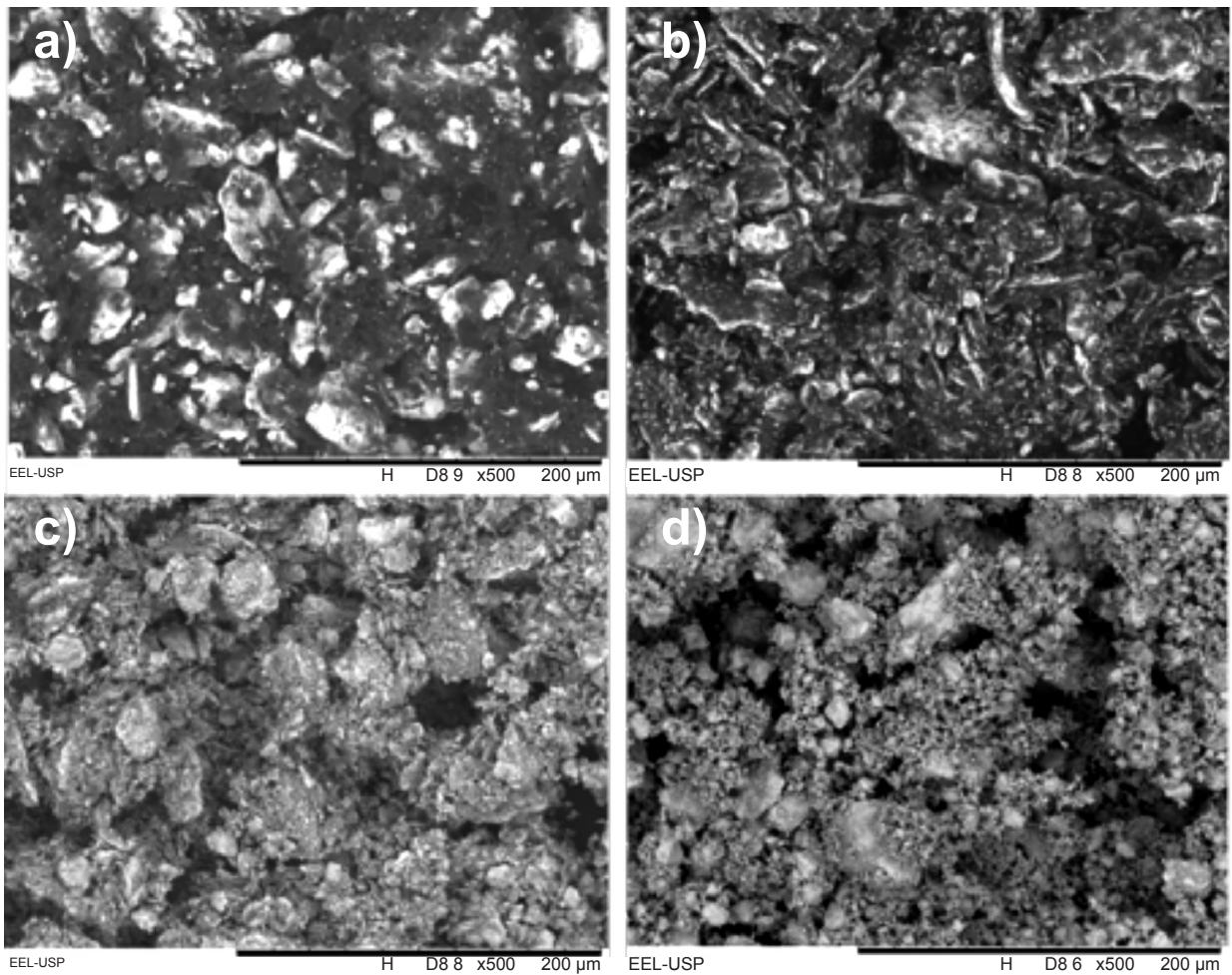

Figure 2: SEM images of W-50C (at%) powders milled at different times: a) 20 min; b) 60 min; c) 180 min; and d) 600 min.
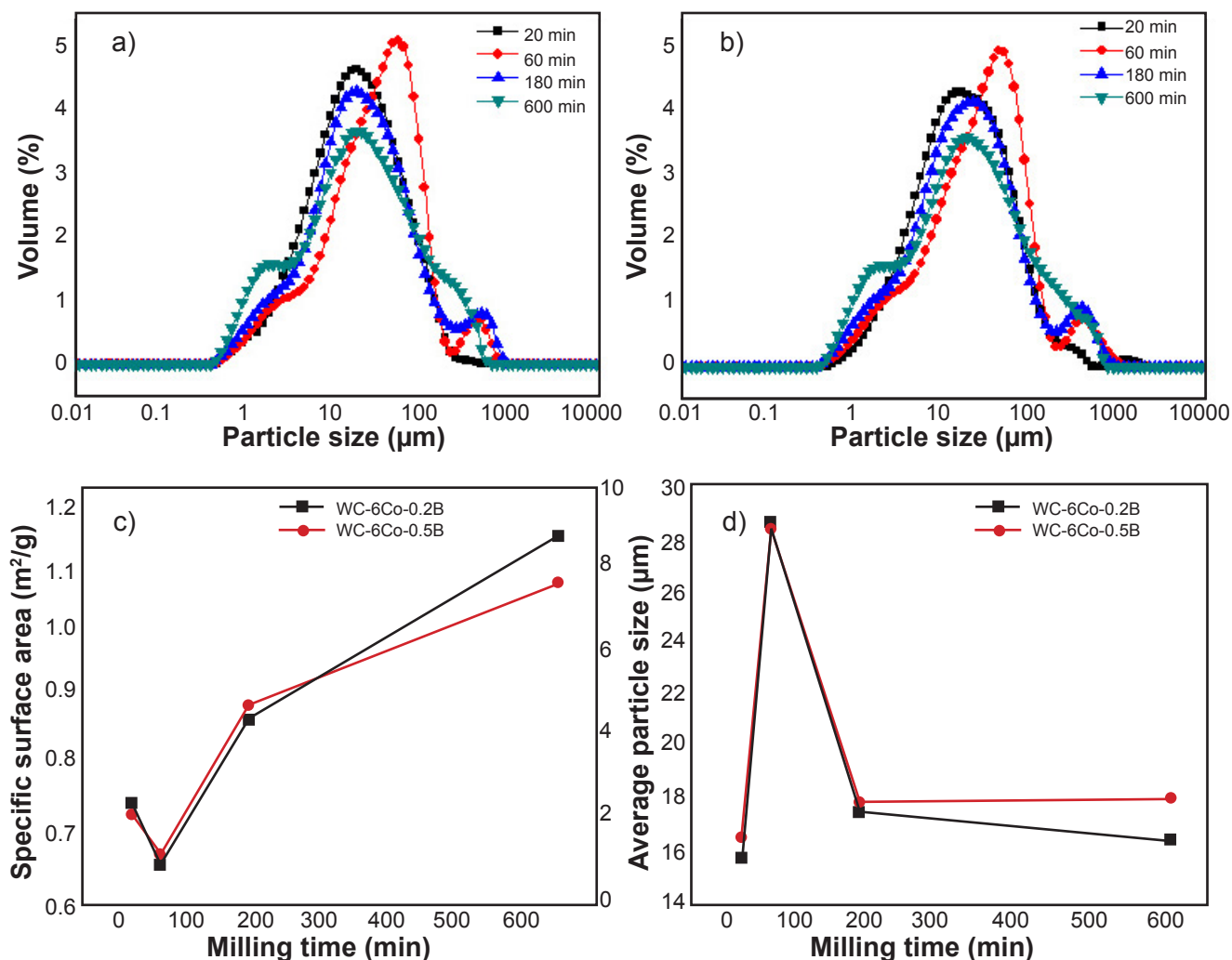
Figure 3: Effect of milling time of W-50C (at%) powder mixtures on the particle size distribution of WC-6Co-0.2B (a) and WC-6Co-0.5B (b), and the specific surface area (c), and average particle size (d) of these powder mixtures.

a flattened morphology was observed in the powders milled for shorter times, Figs. 2a-2c, whereas a high amount of fine particles with a rounded morphology was observed in the powder milled for 600 min (Fig. 2d). Work hardening and solid solution strengthening were not effective in minimizing the cold welding between ductile particles during shorter milling times, whereas the formation of WC particles accentuated the fracture mechanism during the ball milling of W-50C (at%) powders.

Fig. 3 exhibits the curves of the particle size distribution of the WC-6Co-0.2B and WC-6Co-0.5B powder mixtures prepared from the W-50C (at%) powders milled at different times as well as the specific surface area and average particle size of WC-6Co-xB (x= 0.2 and 0.5 wt%) powder mixtures. Modal size distribution was observed in the powder mixtures milled for 20 min, whereas a bimodal size distribution was detected in the powder mixtures milled for longer times. The average particle size of both WC-6Co-0.2B and WC-6Co-0.5B powder mixtures prepared with W-50C powders milled for 60 and 600 min first increased to 28 μm and then decreased to 16-18 μm. The specific surface area of

WC-6Co-0.2B and WC-6Co-0.5B powders increased from 0.7 m²/g (60 min) to 1.1 m²/g (600 min). Therefore, the WC-6Co-0.2B powder mixture had a smaller particle size than the B-rich (0.5 wt%) one.

Characterization of sintered WC-6Co-0.2B and WC-6Co-0.5B ceramic composites: during the SPS process, the nanocrystalline and metastable (C solid solution in W lattice) samples of W-C-Co-B powders were placed in a graphite die, and two electrically-conductive punches were used to create electrical pulses and heat the samples by the Joule effect. A fine graphite-C-rich layer was formed on the surfaces of WC-6Co-0.2B and WC-6Co-0.5B ceramic composites, and its further removal by conventional metallographic techniques was needed. The XRD patterns of the sintered ceramic composites produced with 0.2 and 0.5 wt% B are illustrated in Fig. 4, whereas Fig. 5 shows the phase contents determined by Rietveld refinement in SPSed WC-6Co-xB (x= 0.2 and 0.5 wt%) ceramics. It was noted the presence of intense WC and C-graphite peaks in XRD patterns of spark plasma sintered samples, which were previously prepared with as-milled WC powders at different times (20, 60, 180,
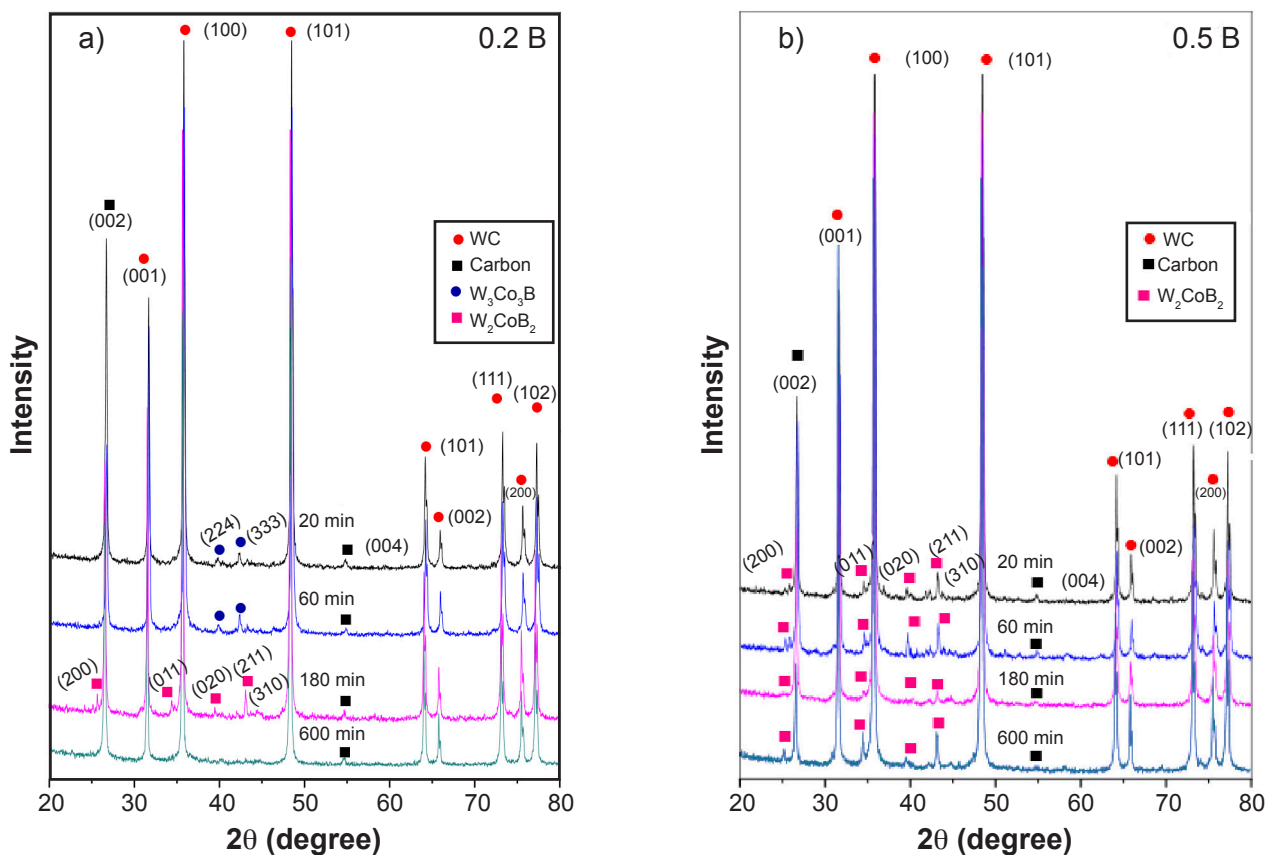
Figure 4: XRD results of WC-6Co-0.2B (a) and WC-6Co-0.5B (b) ceramic composites sintered with as-milled W-50C (at%) powders at different times (20, 60, 180, and 600 min)
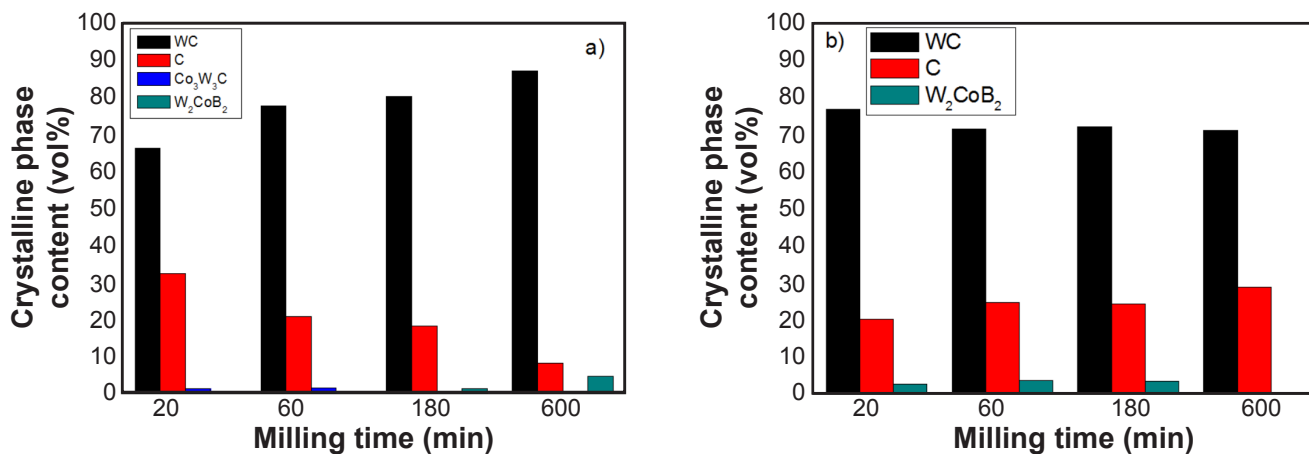

Figure 5: Effect of milling time on phase content determined by Rietveld refinement in SPSed WC-6Co-0.2B (a) and WC-6Co-0.5B (b) ceramics.

and 600 min). Minor peaks of Co_3W_3C (20 and 60 min) and W_2CoB_2 (180 min) were also indexed in XRD patterns of the sintered WC-6Co-0.2B ceramic composite (Fig. 4a). No ternary phase was indexed in the XRD pattern of this ceramic composite produced with W-50C (at%) powders milled for 600 min, which could be associated with the less-reactive nanocrystalline WC powders used as starting materials. Only the peaks of WC, graphite-C and W_2CoB_2 were indexed in the XRD patterns of the sintered WC-6Co-0.5B ceramic composite (Fig. 4b). With the increasing milling

time of W-50C (at%) powders, the WC amount continuously increased, whereas the graphite-C amount of the sintered WC-6Co-0.2B ceramic composite was gradually reduced (Fig. 5a). In order to avoid any adhesion between the punch and the samples, graphite papers were used as spacers, and this phenomenon could be responsible for the presence of C-graphite in the detected XRD patterns [5].

Fig. 6 displays the SEM micrographs of WC-6Co-0.2B and WC-6Co-0.5B ceramic composites produced from the powders milled for 20 and 600 min. These ceramic

composites possessed inhomogeneous microstructures with matrixes formed by coarse (~12 μm) and fine (<3 μm) WC grains [23, 24]. However, the presence of isotropic coarsening without abnormal WC grain growth was detected near W_2CoB_2 and Co_3W_3C precipitates, which were located near WC grain boundaries. Table II shows the results of semi-quantitative analysis by the EDS technique of phases in SPSed WC-6Co-0.2B and WC-6Co-0.5B ceramics produced with W-50C at% powders milled at different times (20 and 600 min). EDS results confirmed that carbon was uniformly distributed in the matrix, whereas boron and cobalt were preferentially located in precipitates and segregated regions. Moreover, the WC grains in the matrix presented similar elemental contents suggesting that the contrast was due to the different crystallography orientations only. In order to support this fact, Fig. 7 shows the EDS spectra containing pronounced Co and B peaks in the precipitate of SPSed WC-6Co-xB (x= 0.2 and 0.5 wt%) samples produced with W-50C at% powders milled for 20 and 600 min. Accordingly, it was noted the presence of Co and B rich regions in the precipitate

of the SPSed WC-6Co-0.5B sample produced with WC-50C at% powders milled for 20 min, which were measured by elemental mapping for carbon, boron, and cobalt in SEM analysis (Fig. 8).

During the SPS process at a low temperature (1450 °C), dense WC-6Co-0.2B and WC-6Co-0.5B ceramic composites were produced from metastable and nanosized WC powders under milling greater than 60 min. The sintered WC-6Co-0.2B ceramic composite had a relative density between 79.7%±0.6% and 86.7%±0.5%, whereas the WC-6Co-0.5B composite exhibited a higher relative density ranging between 86.7%±0.6% and 90.9%±0.4%. On contrary, these sintered ceramic composites previously prepared with nanocrystalline WC powders (after milling for 600 min) indicated lower relative densities close to 82.7%±0.6% and 84.1%±0.5%, respectively. Both the released heat from metastable structures formed by mechanical alloying and high sintering pressures during SPS contributed to the formation of dense WC-based ceramic composites at a low sintering temperature of 1450 °C.
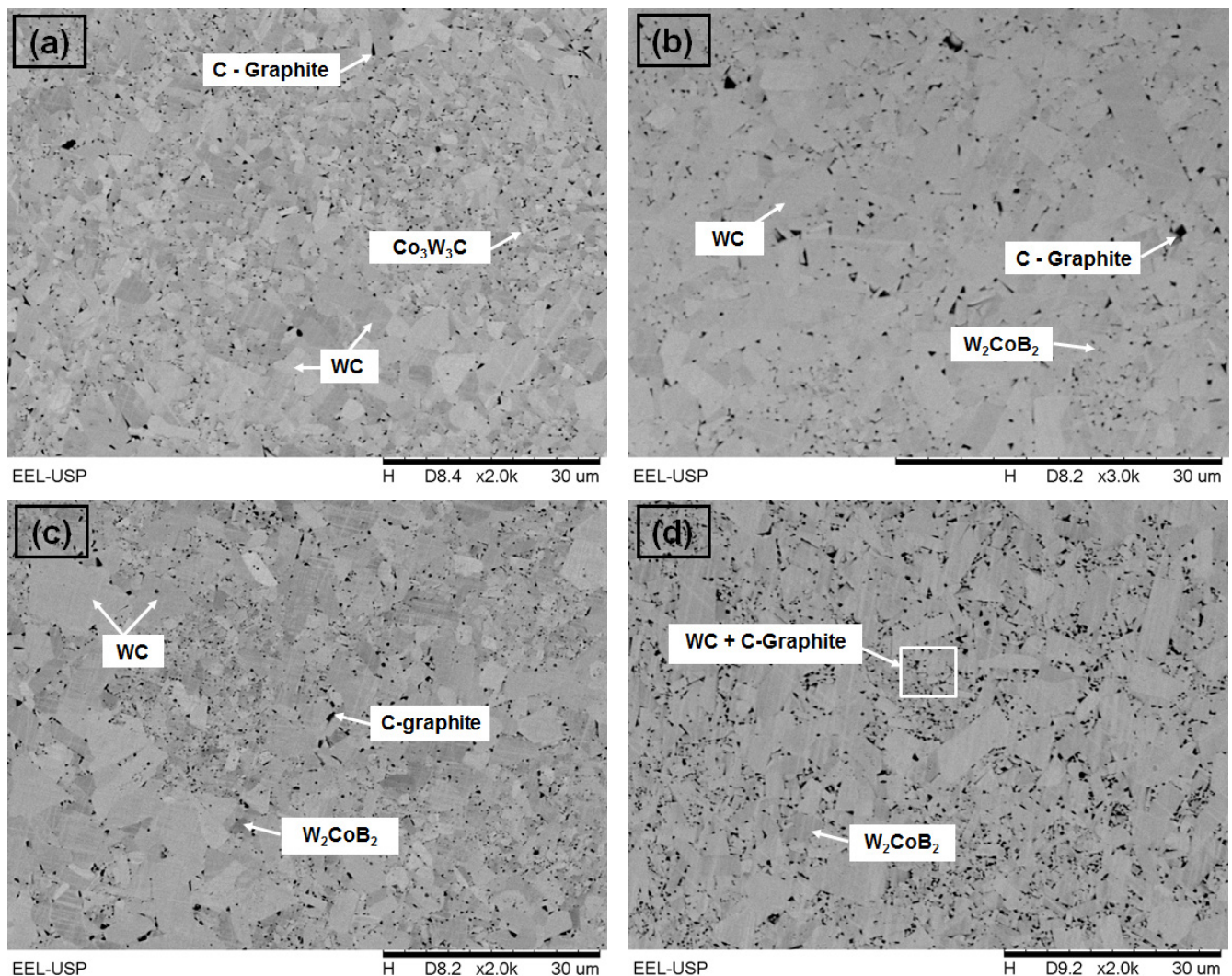

Figure 6: SEM images of sintered WC-6Co-0.2B (a,b) and WC-6Co-0.5B (c,d) ceramics produced with W-50C (at%) powders milled for 20 min (a,c) and 600 min (b,d).

Table II - Results of semi-quantitative analysis by EDS technique of phases in SPSed WC-6Co-0.2B and WC-6Co-0.5B ceramics produced with W-50C at% powders milled at different times (20 min and 600 min).

Sample	Phases	W (at%)	C (at%)	Co (at%)	B (at%)
WC-6Co-0.2B (20 min)	WC-matrix	15.9-35.3	78.2-64.7	5.9-0	-
	WC+precipitate	49.1	33.9	17.0	-
WC-6Co-0.5B (20 min)	WC-matrix	32.4-31.7	67.6-68.3	-	-
	WC+precipitate	48.8-45.3	26.2-33.5	25.0-21.2	-
	Co	1.4 (1.7)	16.0 (0)-19.2	82.6 (98.3)-79.5	-
WC-6Co-0.2B (600 min)	WC-matrix	33.6-34.2	66.4-65.9	-	-
	WC+precipitate	22.3-20.1 (17.7)	77.7-79.9 (74.6)	-	0-(7.6)
WC-6Co-0.5B (600 min)	WC-matrix	32.1-34.7	67.9-65.3	-	-
	WC+precipitate	31.0-27.7	69.1-72.3	-	-

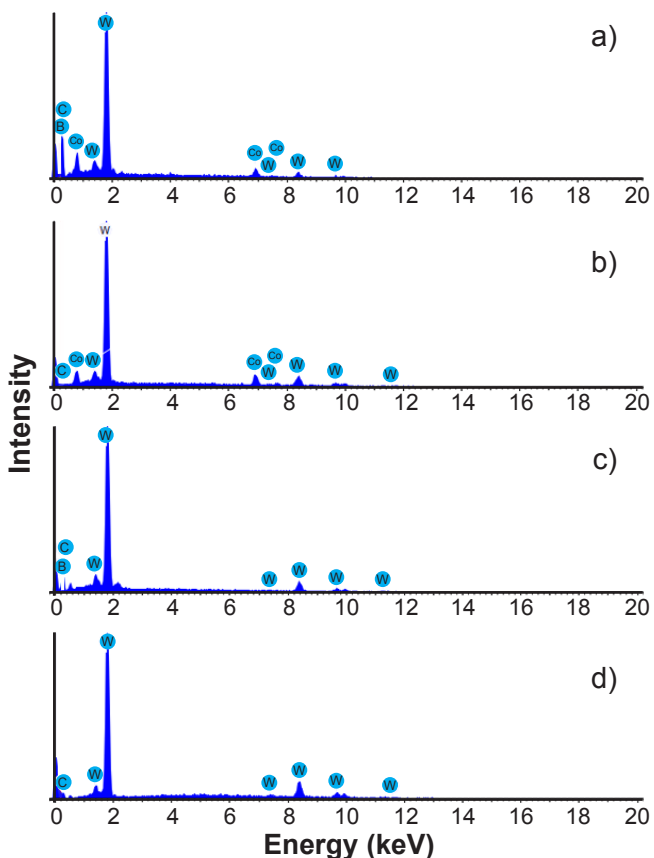*Note: particular measurement given in parentheses.*

Figure 7: EDS spectra of precipitates in WC-6Co-0.2B (a,c) and WC-6Co-0.5B (b,d) ceramics produced with W-50C at% powders milled for 20 min (a,b) and 600 min (c,d).
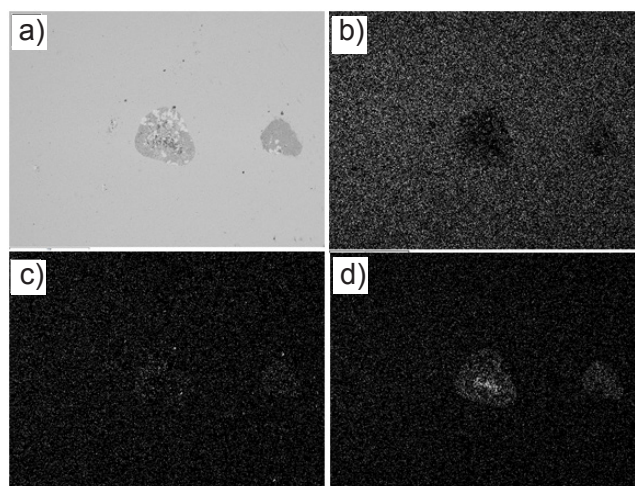

Figure 8: SEM micrograph (a) and EDS elemental mapping images of carbon (b), boron (c), and cobalt (d) of SPSed WC-6Co-0.5B ceramic produced with W-50C at% powders milled for 20 min showing the presence of Co and B rich regions.

Mechanical properties: Vickers hardness values of the sintered WC-6Co-0.2B and WC-6Co-0.5B ceramic composites produced from W-50C at% powders milled for different times are presented in Fig. 9. The Vickers hardness ($HV_{0.5}$) value of the sintered WC-6Co-0.2B ceramic composite varied between 1790±38 HV (17.6±0.4 GPa) and 2158±25 HV (21.2±0.2 GPa), whereas that of the WC-6Co-0.5B ceramic composite ranged between 1858±31 HV (18.2±0.3 GPa) and 2182±28 HV (21.4±0.3

GPa). Therefore, the highest Vickers hardness values of WC-6Co-0.2B and WC-6Co-0.5B ceramic composites were obtained from metastable WC powders milled for 180 and 60 min, respectively, which can be attributed to their higher densification and the formation of W_2CoB_2 with very fine WC grains. The Vickers hardness values of hot-pressed WC-Al$_2$O$_3$ composites reinforced by graphene platelets [39] and spark plasma sintered WC-8Co-0.2VC-1cBN ultrafine-grained cemented carbide [40] were reported as 18.8 and 20.8 GPa, respectively.

Fig. 10 shows the fracture strength obtained in the diametral compression test of sintered WC-Co-B ceramic composites, which were previously prepared at different milling times. It was noted that the WC-6Co-0.2B ceramic composite presented slightly higher fracture strength values than the WC-6Co-0.5B composition at all milling times investigated. However, the high standard deviations measured at different milling times and boron additions hindered such a relationship. In this sense, these values
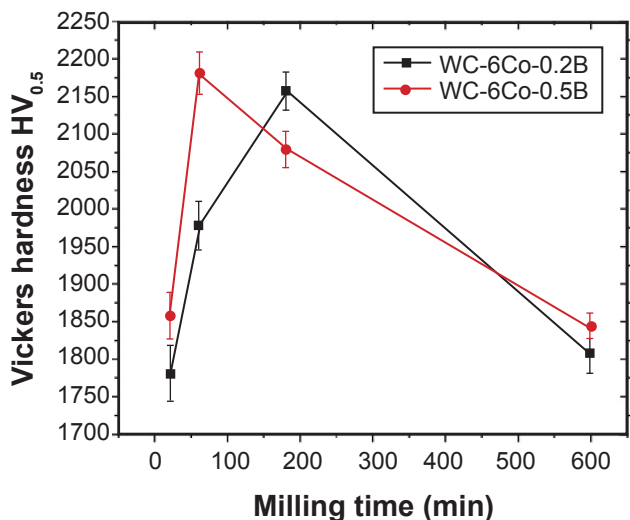
Figure 9: Vickers hardness ($HV_{0.5}$) of sintered WC-6Co-0.2B and WC-6Co-0.5B ceramic composites as a function of milling time of W-50C (at%) powder mixture.
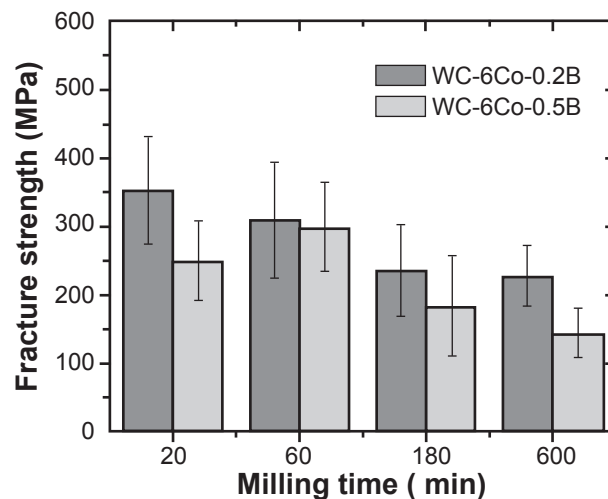

Figure 10: Diametral fracture strength of the sintered WC-6Co-0.2B and WC-6Co-0.5B ceramic composites as a function of milling time of WC powder mixture.
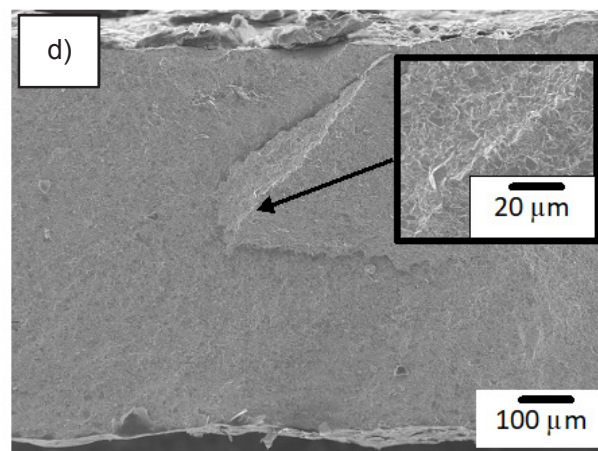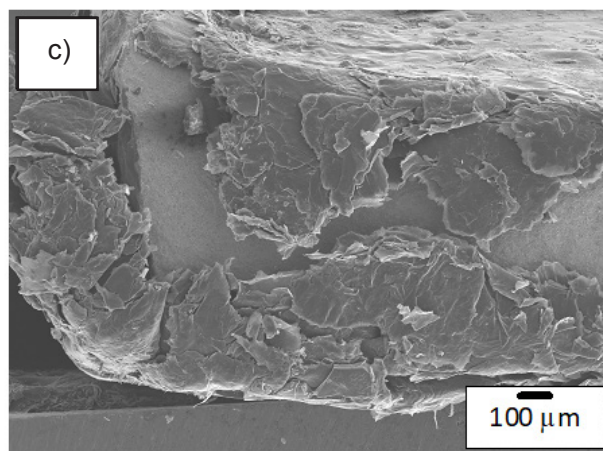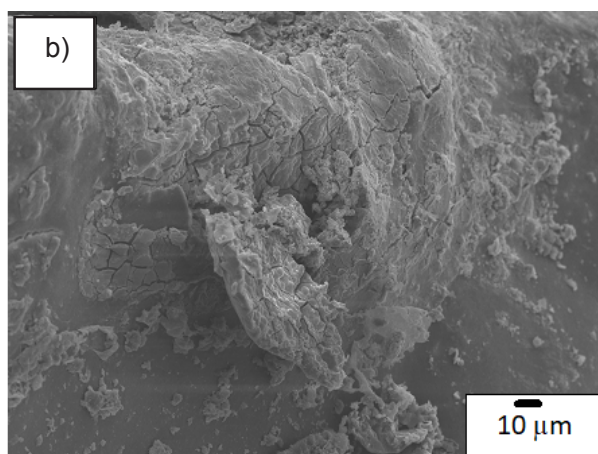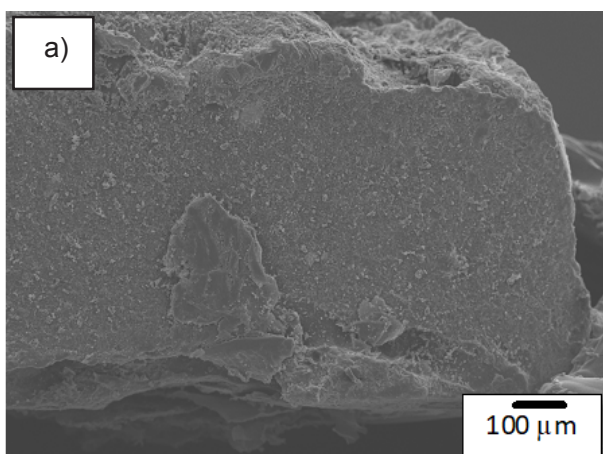

Figure 11: SEM images showing details of fracture surfaces after diametral compression tests of spark plasma sintered WC-6Co-0.2B (a,c) and WC-6Co-0.5B (b,d) ceramic composites prepared with powders milled for 20 min (a,b) and 600 min (c,d).

varied from 353±78 MPa (20 min) to 228±44 MPa (600 min) for WC-6Co-0.2B ceramic composite, whereas they were between 299±65 MPa (60 min) and 144±35 MPa (600 min) for the WC-6Co-0.5B ceramic composite. There was

a tendency for reducing the fracture strength due to the crystallographic changes of the starting powder, as well as in the crystallization of W_2CoB_2. In addition, the formation of WC during milling of W-50C (at%) powders for 600

min also contributed to reducing the released energy gain during sintering from the partially metastable powders. However, the standard deviation values observed denoted a great variation of property, indicating that porosity is the primary factor in determining the mechanical characteristics of composites. Anyway, a very long milling time (600 min) was the condition in which the material had the lowest values of mechanical strength, as well as observed in the hardness of the materials, and can be correlated with the reduction of the relative density of the material, as a result of the reduction of sinterability of these powders during the spark plasma sintering process. The fracture surfaces of the spark plasma sintered WC-6Co-0.2B and WC-6Co-0.5B after diametral compression tests are presented in Fig. 11. The WC-Co-B specimens were fragmented into small pieces during the diametral compression tests, which exhibited little or no evidence of plastic deformation. Independently on composition and milling time, the specimens exhibited a brittle rupture with intergranular fracture (Fig. 11), indicating that the grain boundaries were weakened. Moreover, it was noted the detachment of the outer layer in regions under tensile loading. This behavior was related to the residual porosity present in all samples after sintering, which contributed to the random crack growing during the diametral compression test. Despite the axial loads acting mainly in the WC-based structural components such as cutting tools, rings, and other components in industrial machinery, the transversal loads could be developed for specific plane stress during their applications and, thus, the diametral compression strength needs to be specifically adjusted for the required application. In this way, the WC-6Co-xB (x= 0.2 and 0.5 wt%) ceramic composites processed by SPS at low temperature are able to support diametral compression strength close to 500 MPa.

CONCLUSIONS

The ball milling of the W-50C (at%) powder mixture contributed to the reduction of the W crystallite size and the powder particle size and also to the formation of metastable and nanocrystalline structures, mainly after high milling times adopted in this work. The SPS process at a low temperature (1450 °C for 10 min) produced partially dense WC-6Co-0.2B (relative density <87%) and WC-6Co-0.5B (relative density <91%) structures, indicating the presence of WC as the matrix and graphite-C, Co_3W_3C, and/or W_2CoB_2 as precipitates. A discrete reduction of relative density was noticed in samples sintered with powders containing metastable crystalline WC phase in comparison with a W-C-Co-B solid solution. SPSed WC-6Co-0.2B and WC-6Co-0.5B ceramic composites had Vickers hardness values of 1790-2158 and 1858-2182 HV, respectively, and their fracture strength was lower than 500 MPa. The variation of relative density under certain sintering conditions influenced the mechanical properties of the sintered composites. Therefore, the sintering at 1450 °C, 40 MPa, and dwell time of 10 min adopted in the spark plasma sintering was not sufficient for the diffusional flow to allow complete densification of powders milled for short times using high energy ball milling.

REFERENCES

[1] Z.Z. Fang, X. Wang, T. Ryu, K.S. Hwang, H.Y. Sohn, Int. J. Refract. Hard Met. **27** (2009) 288.
[2] V. Bonache, E. Rayón, M.D. Salvador, D. Busquets, Mater. Sci. Eng. A **527**, 12 (2010) 2935.
[3] H. Klaasen, J. Kubarsepp, Wear **261** (2006) 520.
[4] C. Jia, L. Sun, H. Tang, X. Qu, Int. J. Refract. Hard Met. **25**, 1 (2007) 53.
[5] C.-C. Jia, H. Tang, X.-Z. Mei, F.-Z. Yin, X.-H. Qu, Mater. Lett. **59** (2005) 2566.
[6] Z.-Y. Hu, Z.-H. Zhang, X.-W. Cheng, F.-C. Wang, Y.-F. Zhang, S.-L. Li, Mater. Des. **191** (2020) 108662.
[7] S. Grasso, J. Poetschke, V. Richter, G. Maizza, Y. Sakka, M.J. Reece, J. Am. Ceram. Soc. **96**, 6 (2013) 1702.
[8] A.K.N. Kumar, K. Kurokawa, in "Tungsten carbide: processing and applications", K. Liu (Ed.), InTech, Rijeka (2012) 41530.
[9] W. Liu, X. Song, K. Wang, J. Zhang, G. Zhang, X. Liu, Mater. Sci. Eng. A **499** (2009) 476.
[10] A. Genç, E. Ayas, M.L. Öveçoğlu, S. Turan, J. Alloys Compd. **542** (2012) 97.
[11] E. Ghasali, T. Ebadzadeh, M. Alizadeh, M. Razavi, Ceram. Int. **44** (2018) 10646.
[12] M. Serati, H. Alehossein, D.J. Williams, J. Mech. Phys. Solids **78** (2015) 123.
[13] J. Takagi, M.C. Shaw, CIRP Annals **30** (1981) 53.
[14] S.B. Luyckx, Acta Metall. Mater. **40** (1992) 1623.
[15] T.B. Massalski (Ed.), "Binary alloy phase diagrams", **2**, ASM Int., Mater. Park (1990).
[16] A.E. McHale, H.F. McMurdie, H.M. Ondik (Eds.), "Phase diagrams for ceramists", **10**, Am. Ceram. Soc., Westerville (1994).
[17] A. Fazili, L. Nikzad, M.R. RahimiPour, M. Razavi, E. Salahi, Int. J. Refract. Hard Met. **69** (2017) 189.
[18] B. Huang, W. Xiong, Z. Yao, S. Chen, M. Zhang, Q. Yang, Ceram. Int. **42** (2016) 5291.
[19] P. Siwak, D. Garbiec, T. Nonferr. Metal. Soc. **26** (2016) 2641.
[20] S. Sugiyama, H. Taimatsu, J. Eur. Ceram. Soc. **24** (2004) 871.
[21] W. Su, Y. Wen, Q. Zhang, Int. J. Refract. Hard Met. **70** (2018) 176.
[22] Z. Huang, X. Ren, M. Liu, C. Xu, H. Chen, Int. J. Refract. Hard Met. **62** (2017) 155.

[23] Q. Yang, J. Yang, H. Yang, J. Ruan, Ceram. Int. **42** (2016) 18100.

[24] A.K.N. Kumar, M. Watabe, K. Kurokawa, Vacuum **88** (2013) 88.

[25] P. Goeuriot, F. Thevenot, N. Bouaoudja, G. Fantozzi, Ceram. Int. **13** (1987) 99.

[26] F. Cardarelli, *Materials handbook: a concise desktop reference*, Springer (2008).

[27] G.S.A. Silva, R.M.L. Neto, V.A.R. Henriques, C.A.A. Cairo, A.S. Ramos, Mater. Sci. Forum **899** (2017) 9.

[28] "Powder diffraction file (inorganic phases)", **2**, JCPDS-ICDD, Swarthmore (1988).

[29] J. Rodriguez-Carvajal, Commission Comm. Powder Diffr. Newslett. **26** (2001) 12.

[30] B962-14, "Standard test methods for density of compacted or sintered powder metallurgy (PM) products using Archimedes' principle", ASTM Int., West Conshohocken (2014).

[31] E384-17, "Standard test method for microindentation hardness of materials", ASTM Int., West Conshohocken (2017).

[32] NBR 7222:2011, "Argamassas e concretos: determinação da resistência à tração por compressão diametral de corpos de prova cilíndricos", ABNT (2011).

[33] D3967-16, "Standard test method for splitting tensile strength of intact rock core specimens", ASTM Int., West Conshohocken (2016).

[34] J.S. Shah, M.E. Straumanis, J. Appl. Phys. **42** (1971) 3288.

[35] Y.X. Zhao, I.L. Spain, Phys. Rev. B **40** (1989) 993.

[36] W.F. Scholosser, Phys. Status Solidi A **17** (1973) 199.

[37] W. Rieger, H. Nowotny, F. Benesovsky, Monatsh. Chem. **97** (1966) 378.

[38] E. Lugscheider, H. Reimann, R. Pankert, Z. Metallkd. **73** (1982) 321.

[39] X. Zhang, S. Zhu, H. Ding, Y. Bai, P. Di, Int. J. Refract. Hard Met. **82** (2019) 81.

[40] Z. Wang, Y. Liu, K. Liu, B. Wang, Ceram. Int. **45** (2019) 23658.